

Non-equilibrium dynamics of dipolar polarons

Artem G. Volosniev¹, Giacomo Bighin^{1,2}, Luis Santos³, Luis A. Peña Ardila^{3,4,†}

1 Institute of Science and Technology Austria (ISTA), Am Campus 1, 3400 Klosterneuburg, Austria

2 Institut für Theoretische Physik, Universität Heidelberg, D-69120 Heidelberg, Germany

3 Institut für Theoretische Physik, Leibniz Universität Hannover, Germany

4 School of Science and Technology, Physics Division, University of Camerino, Via Madonna delle Carceri, 9B - 62032 (MC), Italy.

* artem.volosniev@ist.ac.at

† luis.penaardila@unicam.it

May 30, 2023

Abstract

We study the out-of-equilibrium quantum dynamics of dipolar polarons, i.e., impurities immersed in a dipolar Bose-Einstein condensate, after a quench of the impurity-boson interaction. We show that the dipolar nature of the condensate and of the impurity results in anisotropic relaxation dynamics, in particular, anisotropic dressing of the polaron. More relevantly for cold-atom setups, quench dynamics is strongly affected by the interplay between dipolar anisotropy and trap geometry. Our findings pave the way for simulating impurities in anisotropic media utilizing experiments with dipolar mixtures.

Contents

1	Introduction	2
2	System	3
3	Variational ansatz	4
4	Results	5
4.1	Steady state	5
4.2	Ramsey contrast	5
4.3	Homogeneous case	6
4.4	Anisotropy of time evolution	8
4.5	Trapped system	9
4.6	Outlook	11
A	On the accuracy of the Fröhlich Hamiltonian	11
B	Static properties of the system	12
C	Derivation of contrast	16
D	Energy for a system in a trap	17
	References	19

1 Introduction

Non-equilibrium dynamics is one of the most challenging and complex branches of quantum many-body physics. It is ubiquitous in several physical systems and is characterized by the interplay between few- and many-body correlations [1, 2]. While few-body processes are important at the initial stages, collective excitations build the subsequent time evolution. Studies of these limits shed light onto far-from-equilibrium processes, particularly on the relevant timescales. A paradigmatic testbed for such studies is a system with an impurity interacting with a quantum environment whose steady-state solution – a polaron [3] – provides a physical intuition behind low-energy transport in semiconductors [4], colossal magnetoresistance [5], non-equilibrium phenomena such as quantum heat transport [6] as well as polaron pairs in semiconducting organic polymers [7]. Unfortunately, it appears challenging to experimentally resolve time dynamics of the polaron in solid state systems, where natural time scales are ‘fast’, given by femtoseconds (for electrons) and picoseconds (for lattice).

To study short-time polaron physics, one can use ultracold quantum gases instead [8, 9], where, depending on the nature of the particles in the bath, impurities can form Bose [10–13] or Fermi polarons [14–17]. Recent cold-atom experiments unveil the relevant time scales of polaron formation by measuring the Ramsey contrast. The initial short-time dynamics of the impurity provided insight into how many-body correlations are built from the few-body level and how excitations dissipate into the bath due to dephasing. On the theoretical side, non-equilibrium dynamics can be studied using several robust approaches based upon variational coherent ansatz [18–20], T-matrix approximation [21], diagrammatic techniques [22], master equation [23, 24], dynamical variational ansatz [25], exact results [26]. However, experimental and theoretical work on non-equilibrium polaron dynamics is so far limited to ultracold gases with short-range interactions. The connection between the far-from-equilibrium dynamics and the equilibrium polaron state remains an open problem for more complicated interactions.

Due to the comparable length scales, namely the range of the potential being on the same order as the interparticle distance, the static properties of impurities with long-range interactions are distinctly different from those for short-range interactions. For example, Rydberg [27, 28] and ionic impurities [29, 30]¹ are dressed by many atoms and form many-body bound states for strong interactions, which are beyond the so-called Fröhlich Hamiltonian. Another scenario is provided by an impurity in a dipolar gas [31, 32] where both the atom-atom and impurity-atom potentials are characterized by a long-range and anisotropic dipole-dipole interaction (DDI). The experimentally relevant interaction regimes of this system can be described using the Fröhlich Hamiltonian, making the dipolar polaron model an ideal platform for simplified theoretical studies of non-equilibrium dynamics in beyond-contact-interaction polaron models.

Motivated by the realization of bosonic mixtures of non-magnetic and magnetic atoms such as Er-Li [33] and Yb-Er [34] as well as of magnetic atoms such as Er and Dy [35–37], in this work, we study non-equilibrium physics of dipolar polarons, i.e., impurities (non-dipolar or dipolar) immersed in a Bose bath with dominant DDI. In stark contrast to systems ruled by short-range

¹In the Rydberg case, the effective impurity-atom potential contains both s - and p - wave scattering terms. For a charged impurity, the potential has an isotropic $1/r^4$ tail.

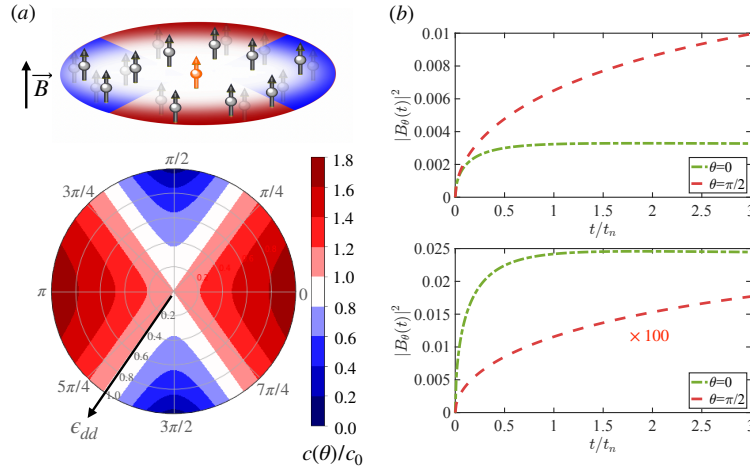


Figure 1: **(a)** Speed of sound $c(\theta)$ for different strengths of dipolar coupling, ϵ_{dd} , depending on the relative direction between the phonon's momentum and the direction of the magnetic field, \vec{B} , which fixes the orientation of the dipoles; c_0 is the speed of sound for a non-dipolar system. **(b)** Population of phonons excited by the impurity in two directions with respect to the impurity. For $\theta = 0$ ($\theta = \pi/2$), the momentum of phonons is parallel (perpendicular) to the direction of the dipoles. The top plot is for a non-dipolar impurity ($d_2 = 0$). The bottom plot is for a dipolar impurity with $d_2 = 130a_0$ (a_0 is the Bohr radius). We consider a homogeneous gas with $na_{11}^3 = 5 \times 10^{-5}$ and $a_{11} = a_{12} = 150a_0$ so that $\epsilon_{dd} \simeq 0.87$. ϵ_{dd} is the parameter that characterizes the dipolar character of the bath, see the text for details.

interactions, the dispersion relation in dipolar systems displays an anisotropic behavior at low energies [38, 39], supporting, for certain parameters, exotic states of matter such as quantum droplets and supersolids [40, 41]. As we shall demonstrate, the anisotropy of dipolar interactions also plays an important role in our study.

To investigate the quench dynamics of the impurity, we rely on a variational ansatz. It allows us to unveil the relevant time scales of the polaron formation and investigate its anisotropic character by computing the contrast – the overlap between the non-interacting and the interacting states. For a non-dipolar impurity, our findings can be observed experimentally using well-established interferometric techniques such as many-body Ramsey spectroscopy see, e.g., [8, 9] or by driving Rabi oscillations between weakly and strongly interacting states [42]. In contrast, for the fully dipolar case, further decoherence processes due to fast dipolar relaxation may play a role.

2 System

We consider a highly imbalanced dipolar binary mixture at zero temperature. We first focus on a uniform three-dimensional system, see Sec. 4.5 for a discussion of an experimentally relevant trapped gas. The problem is cast in the framework of a single impurity problem interacting with a dipolar condensate. The host bath is labeled by $|1\rangle$ with density n and the impurity is labeled by $|2\rangle$. For equal mass components, $m_1 = m_2 = m$, the out-of-equilibrium dynamics of the impurity obeys the Fröhlich Hamiltonian,

$$\hat{\mathcal{H}} = \sum_{\mathbf{k}} \omega_{\mathbf{k}} \hat{b}_{\mathbf{k}}^\dagger \hat{b}_{\mathbf{k}} + \frac{\hat{\mathbf{P}}^2}{2m} + nV_{12}(\mathbf{k} = 0) + \frac{\sqrt{n}}{\sqrt{V}} \sum_{\mathbf{k}} V_{12}(\mathbf{k}) W_{\mathbf{k}} e^{-i\mathbf{k} \cdot \hat{\mathbf{r}}} \left(\hat{b}_{\mathbf{k}} + \hat{b}_{-\mathbf{k}}^\dagger \right), \quad (1)$$

which describes the scattering between an impurity with momentum operator $\hat{\mathbf{P}}$ and a Bogoliubov bosonic excitation of energy $\hbar\mathbf{k}$. Here, $\hat{b}_{\mathbf{k}}$ ($\hat{b}_{\mathbf{k}}^\dagger$) annihilates (creates) an excitation with energy $\omega_{\mathbf{k}} = \sqrt{\epsilon_{\mathbf{k}}(\epsilon_{\mathbf{k}} + 2nV_{11}(\mathbf{k}))}$ where $\epsilon_{\mathbf{k}} = \hbar^2\mathbf{k}^2/2m$ is the free energy dispersion, and $W_{\mathbf{k}} = \sqrt{\epsilon_{\mathbf{k}}/\omega_{\mathbf{k}}}$. The boson-boson (V_{11}) and impurity-boson (V_{12}) potentials are given by $V_{ij}(\mathbf{k}) = g_{ij} + g_{ij}^d (3k_z^2/\mathbf{k}^2 - 1)$. The first term of this expression describes the short-range physics characterized by the coupling strength g_{ij} , which within the Born approximation reads $g_{ij} = 4\pi\hbar^2 a_{ij}/m$ where a_{ij} is the s -wave scattering length. The second part contains the long-range DDI potential, which is anisotropic. Its strength is determined by the dipolar coupling strength $g_{ij}^d = \mu_0\mu_i\mu_j/3 = 4\pi\hbar^2\sqrt{d_i d_j}/m$, where μ_0 is the vacuum permeability, and $\mu_{i(j)}$ is the magnetic dipolar moment related to the dipolar length $d_{i(j)}$.

The anisotropy of the DDI implies that the velocity of Bogoliubov excitations depends on the direction [43]. Figure 1 depicts the anisotropic speed of sound $c(\theta)/c_0 = \sqrt{1 + \epsilon_{dd}(3\cos^2\theta - 1)}$, where $\epsilon_{dd} = d_1/a_{11}$ is the ratio between the dipolar and scattering lengths of the bath, and $c_0 = \sqrt{g_{11}n/m}$ is the sound velocity for the isotropic non-dipolar case ($d_1 = 0$). The velocity $c(\theta)$ is approximately inversely proportional to the relaxation time driven by the low-energy excitations in the condensate. Relaxation takes longer in the side-to-side ($\theta = \pi/2$) direction than in the head-to-tail ($\theta = 0$) one, see Fig. 1. The number of excited bosons is also direction-dependent. Note that excitations with momentum perpendicular to the direction of dipoles ($\theta = \pi/2$) may be unstable [43], i.e., the speed of sound may become imaginary, which leaves a trace in the dynamics of the impurity, as we show below.

To conclude the problem formulation, let us motivate the use of the Fröhlich approximation, which is expected to be accurate only for weak interactions. As our focus is on the dynamics and decoherence of the impurity due to the interplay between the short and long-range anisotropic physics, we shall only explore systems with $a_{ij} \simeq d_i$, i.e., the s -wave scattering length that determines the short-range physics is comparable to the dipolar length of magnetic atoms. For Dy, $d_1 \simeq 130a_0$, which for experimentally relevant densities implies a small gas parameter ($na_1^3 \ll 1$), allowing us to use the Fröhlich Hamiltonian as long as $\epsilon_{dd} < 1$, see also App. A.

3 Variational ansatz

To investigate the out-of-equilibrium dynamics of the system, we employ a coherent-state variational ansatz [18–20, 44] for the wave function $|\psi(t)\rangle = e^{-i\phi(t)} e^{\sum_{\mathbf{k}} \beta_{\mathbf{k}}(t) \hat{b}_{\mathbf{k}}^\dagger - \beta_{\mathbf{k}}^*(t) \hat{b}_{\mathbf{k}}} |0\rangle$. Here, $|0\rangle = |0_{\mathbf{k}}, \mathbf{P}\rangle$ is the state of the system at $t = 0$, which consists of an impurity with momentum \mathbf{P} and a phononic vacuum². The parameters $\beta_{\mathbf{k}}(t)$ and $\phi(t)$ are calculated using the standard principles of time-dependent variational theory, which minimizes the action functional $\int dt \langle \psi(t) | i\hbar\partial_t - \hat{\mathcal{H}} | \psi(t) \rangle$ [45] with the Hamiltonian after the Lee-Low-Pines transformation [46], $\hat{\mathcal{H}} = \hat{S}^{-1} \hat{\mathcal{H}} \hat{S}$ and $\hat{S} = \exp(i\hat{\mathbf{r}} \cdot \hat{\mathbf{P}}_B)$. The corresponding equations for $\beta_{\mathbf{k}}(t)$ and $\phi(t)$ read

²As we show below $\sum_{\mathbf{k}} |\beta_{\mathbf{k}}|^2 \rightarrow 0$ for weak impurity-boson interactions (i.e., $V_{12} \rightarrow 0$), which implies that $e^{\sum_{\mathbf{k}} \beta_{\mathbf{k}}(t) \hat{b}_{\mathbf{k}}^\dagger - \beta_{\mathbf{k}}^*(t) \hat{b}_{\mathbf{k}}} \simeq 1 + \sum_{\mathbf{k}} [\beta_{\mathbf{k}}(t) \hat{b}_{\mathbf{k}}^\dagger - \beta_{\mathbf{k}}^*(t) \hat{b}_{\mathbf{k}}]$. Therefore, the coherent-state variational ansatz in our calculations corresponds (approximately) to an ansatz based upon a single-phonon excitation. This means that our steady-state results should be accurate at the level of second-order perturbation theory where perturbation is given by V_{12} , see also App. B.

$$i\hbar\dot{\beta}_{\mathbf{k}} = \frac{\sqrt{n}}{\sqrt{V}}V_{12}(\mathbf{k})W_{\mathbf{k}} + \Omega_{\mathbf{k}}\beta_{\mathbf{k}}, \quad (2)$$

$$\hbar\dot{\phi}(t) = V_{12}(\mathbf{0})n + \frac{\mathbf{P}^2 - \mathbf{P}_B^2}{2m} + \frac{\sqrt{n}}{\sqrt{V}} \sum_{\mathbf{k}} W_{\mathbf{k}} V_{12}(\mathbf{k}) \Re[\beta_{\mathbf{k}}],$$

where $\Omega_{\mathbf{k}} = \omega_{\mathbf{k}} + \epsilon_{\mathbf{k}} - \hbar\mathbf{k}(\mathbf{P} - \mathbf{P}_B)/m$. The momentum of the bosons, $\mathbf{P}_B = \sum_{\mathbf{k}} \hbar\mathbf{k} |\beta_{\mathbf{k}}|^2$, will be neglected in our calculations (see below). In addition, we note that Eq. (2) should be regularized (see the discussion in App. B).

4 Results

4.1 Steady state

First, we study static properties of the system with $\mathbf{P} = 0$, by imposing in Eq. (2) the saddle-point condition, i.e., $\dot{\beta}_{\mathbf{k}} = 0$. The corresponding solution is $\beta_{\mathbf{k}} = -\sqrt{n}V_{12}(\mathbf{k})W_{\mathbf{k}}/(\sqrt{V}\Omega_{\mathbf{k}})$. Note that $\beta_{\mathbf{k}}$ is proportional to $V_{12}(\mathbf{k})$, thus, \mathbf{P}_B enters in the next-to-leading order (hierarchy is determined by powers of V_{12}). Therefore, \mathbf{P}_B should not be considered when investigating the leading order effect, validating the neglect of \mathbf{P}_B above. We turn at this point to the equation of motion for the phase ϕ . We identify the polaron energy as $E_0 = \hbar\dot{\phi}(t)$, leading to $E_0 = V_{12}^{\Lambda}n - \frac{n}{V} \sum_{\mathbf{k}}^{\Lambda} \frac{(V_{12}(\mathbf{k})W_{\mathbf{k}})^2}{\omega_{\mathbf{k}} + \epsilon_{\mathbf{k}}}$. The first term here corresponds to the mean-field result, whereas the second one includes quantum fluctuations at the level of second-order perturbation theory. Note that we employed the regularized potential $V_{12}^{(\Lambda)} = \frac{4\pi\hbar^2}{m} \left[a_{12} + d_1 d_2 \frac{8}{5\pi} \Lambda + \frac{2a_{12}^2}{\pi} \Lambda \right]$, where Λ is a high-energy cut-off parameter. For a more detailed discussion of a steady state and $V_{12}^{(\Lambda)}$, see App. B.

4.2 Ramsey contrast

We are interested in time evolution that follows an immersion of the impurity in the bath. This corresponds to an abrupt quench of V_{12} from zero to a finite value. For a non-dipolar impurity, this change can be realized using known experimental protocols, see, e.g., [9]. For a dipolar impurity, this could be done by first embedding the dipolar particle initially in the non-magnetic $m = 0$ state, at a magnetic field such that $a_{12} = 0$, and then transferring the impurity to the (maximally stretched) magnetic state of lowest Zeeman energy. This procedure would also result in this case to the desired abrupt switching-on of V_{12} .

To illustrate time evolution, we evaluate the contrast, i.e. the overlap between the polaron wave function and the initial state, $S(t) = \langle \psi(0) | \psi(t) \rangle$. Note that $S(t)$ does not contain any information about the directional dependence of the dynamics. It is an experimentally relevant observable that contains only the information averaged over the sample. For the coherent variational ansatz, the contrast takes a simple form

$$S(t) = \exp \left[-i\phi(t) + \frac{1}{2} \sum_{\mathbf{k}} |\beta_{\mathbf{k}}(t)|^2 \right]. \quad (3)$$

Using it and Eq. (2), we derive a semi-analytical expression:

$$S(t) = \exp \left[-\frac{iE_0 t}{\hbar} + \frac{4i}{3} \sqrt{\frac{na_{11}^3}{\pi}} \left(\frac{a_{12}}{a_{11}} \right)^2 \mathcal{R} \left(\frac{t}{t_n} \right) \right], \quad (4)$$

where the dipolar character of the problem is incorporated in E_0 and \mathcal{R} :

$$\mathcal{R}(x) = \int_0^1 du z(u)^2 \left\{ x \sqrt{w(u)} + e^{\frac{ixw(u)}{2} + \frac{i\pi}{4}} \sqrt{\frac{\pi x}{2}} (3i - w(u)x) \operatorname{erfc} \left[\frac{1+i}{2} \sqrt{xw(u)} \right] \right\},$$

and E_0 is the steady-state polaron energy, which can be conveniently written as $E_0 = g_{12}n + \gamma \int du z(u)^2 w(u)^{1/2}$ where $\gamma \sim (na_{11}^3)^{3/2}$ is presented in App. B; $z(u) = 1 + \frac{\sqrt{d_1 d_2}}{a_{12}} (3u^2 - 1)$ and $w(u) = 1 + \epsilon_{dd} (3u^2 - 1)$ are auxiliary functions; $t_n = \frac{m}{8\pi n \hbar a_{11}}$ is the characteristic timescale, see App. C.

The short-time dynamics ($t \ll t_n$) of the contrast follows from Eq. (4)³

$$S(t) \approx 1 - (1+i) \sqrt{\frac{t}{t_\Omega}} - i \frac{ng_{12}}{\hbar} t, \quad (5)$$

where the initial dynamics is characterized by the timescale

$$t_\Omega = \frac{m}{32\pi \hbar n^2 (a_{12}^2 + \frac{4}{5}d_1 d_2)^2}, \quad (6)$$

which is determined by low-energy two-body impurity-boson scattering. Our approach does not allow us to access the unitarity-limited universal dynamics [9, 47]. These dynamics can however be observed in current experiments only with strongly interacting gases making it irrelevant for our study.

At long times $t \gg t_n$, the phase and the absolute value of the contrast approach the steady-state quantities: the polaron energy E_0 and the quasiparticle residue, $Z = |S(t \rightarrow \infty)|$, which is given by

$$Z = \exp \left[-\frac{8}{3} \sqrt{\frac{na_{11}^3}{\pi}} \left(\frac{a_{12}}{a_{11}} \right)^2 \int_0^1 \frac{z(u)^2}{\sqrt{w(u)}} du \right]. \quad (7)$$

To illustrate the time evolution of the contrast for intermediate times, we shall first consider the system in a box potential, for which the density of the Bose gas is uniform.

4.3 Homogeneous case

We consider the scenario where $a_{11} \gtrsim d_1$, which corresponds to a stable system with dynamics strongly affected by dipole-dipole interactions. At $t < 0$, $V_{12} = 0$; at $t = 0$, the impurity-bath interaction is turned on, initiating the quench dynamics. Figure 2 (a) depicts the amplitude and phase of the contrast as a function of time for a typical gas parameter $na_{11}^3 = 5 \times 10^{-5}$. Following Refs. [9, 48], we distinguish two regimes of the dynamics, namely, the two-body ‘‘relaxation’’ and the many-body ‘‘polaron formation’’, which for a non-dipolar impurity can be accessed experimentally by using interferometric techniques. During the initial ‘‘relaxation’’, which occurs for $t \ll t_n$, mainly two-body collisions between the impurity and the bath are relevant. Such two-body processes dominate the dynamics for times on the order of tenths of μs for typical experimental conditions.

In Fig. 2 (b), we present the time evolution of the contrast (4), and the instantaneous energy, defined as $E = \hbar \dot{\phi}$. In the ‘‘relaxation’’ regime, the energy of the system decreases as a function of time due to the energy exchange (dephasing) with the bosonic bath. For $t \sim t_n$, the system is in the

³Note that we disregard the term $i \frac{t}{t_\Omega}$, which is proportional to V_{12}^4 for consistency of our derivations. Note also that the quantum fluctuations term, $\sim \gamma \int_0^1 du z(u)^2 \sqrt{w(u)} t$, drops out in the expression. It becomes relevant only at longer time scales.

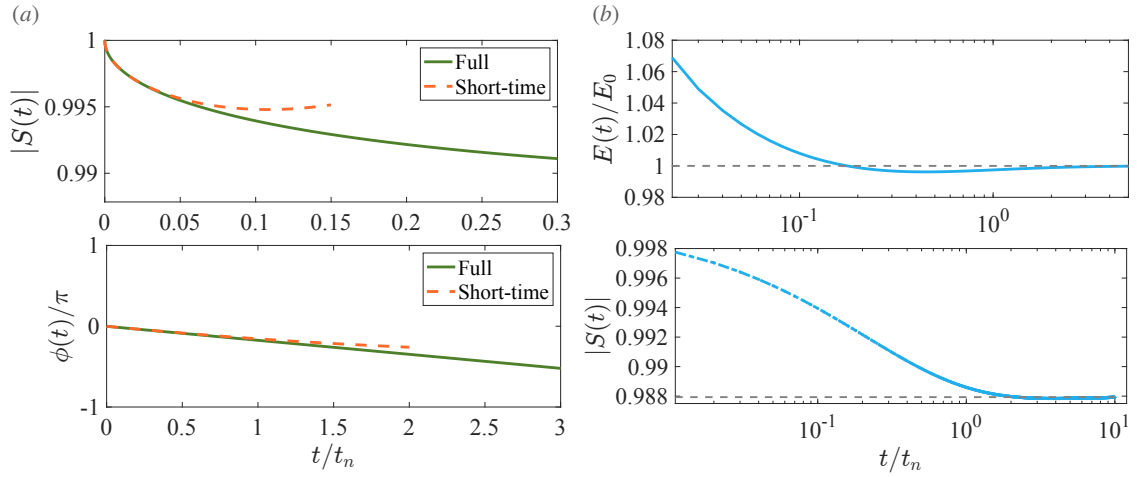


Figure 2: Dipolar polaron contrast (a) Absolute value and phase of the contrast (solid green curves) together with the corresponding short-time prediction of Eq. (5) (dashed orange curves) for a homogeneous dipolar quantum gas. (b) Instantaneous energy $E(t)$ and amplitude of the contrast as a function of time (solid blue curves); E_0 is the polaron energy in the steady state; $|S(t \rightarrow \infty)|$ converges to the quasiparticle residue Z [Eq. (7)], which is shown with a dashed gray line. Note that the formation of the polaron occurs on time scales given by t_n . Here we used the gas parameter $na_{11}^3 = 5 \times 10^{-5}$; the coupling strengths are $d_1 = d_2 = 130a_0$, $\epsilon_{dd} = 0.993$ and $a_{12} = a_{11}$. The time scales t_n and t_Ω for these parameters and for Dy atoms are approximately 0.1ms and 0.2s.

“formation” region where collective excitations of the Bose gas are building up the quasiparticle. For $t \gg t_n$ the polaron is formed – its instantaneous energy is the steady-state energy of the polaron; the absolute value of the contrast is the quasiparticle residue.

In Fig. 3 (a), we plot $|S(t)|$ as a function of time for different values of $\epsilon_{dd} < 1$ (recall that for $\epsilon_{dd} = 1$ the system is unstable against 3D collapse). Firstly, we consider the case $a_{11} = a_{12}$. We tune ϵ_{dd} by changing a_{11} for fixed $d_1 = d_2$. For $a_{11} = a_{12}$ and $d_1 = d_2$, the boson-boson and boson-impurity interactions as well as the functions $z(u)$ and $\omega(u)$ are identical. This implies values of the residue close to unity even for $\epsilon_{dd} \rightarrow 1$, see Eq. (7). As ϵ_{dd} decreases, i.e., the bath becomes less dipolar, the quasiparticle residue also decreases. This happens due to the increase of a_{11} , which makes the bath more strongly interacting, rendering the dynamics *less* coherent.

In Fig. 3 (b), we present $|S(t)|$ for $a_{11} = 2a_{12}$. In this case, the residue vanishes as $\epsilon_{dd} \rightarrow 1$ due to a slow logarithmic divergence of the integral in Eq. (7). Vanishing residue leads to a number of differences in comparison to the previously discussed symmetric case. In particular, for $\epsilon_{dd} \approx 1$, the absolute value of the contrast approaches the result of Eq. (7) at timescales much longer than the typical timescales of polaron formation, $t \simeq t_n$. By analyzing the function $R(t/t_n)$, we conclude that for $\epsilon_{dd} \approx 1$ long-time dynamics of the contrast is of the form

$$|S(t)| \simeq Z \exp \left[-\sqrt{\frac{na_{11}^3}{27\pi}} \left(\frac{4t_n(a_{12} - \sqrt{d_1 d_2})}{t(1 - \epsilon_{dd})a_{11}} \right)^2 \right], \quad (8)$$

which allows us to introduce a relevant timescale close to the collapse: $t_\epsilon = t_n/(1 - \epsilon_{dd})$; Eq. (8) is valid for $t \gg t_\epsilon$ and $\sqrt{d_1 d_2} \neq \epsilon_{dd} a_{12}$. The timescale t_ϵ underlies the very slow dynamics of $|S(t)|$ and of the instantaneous polaron energy as $\epsilon_{dd} \rightarrow 1$. We illustrate this slowdown in the inset of Fig. 3 (b).

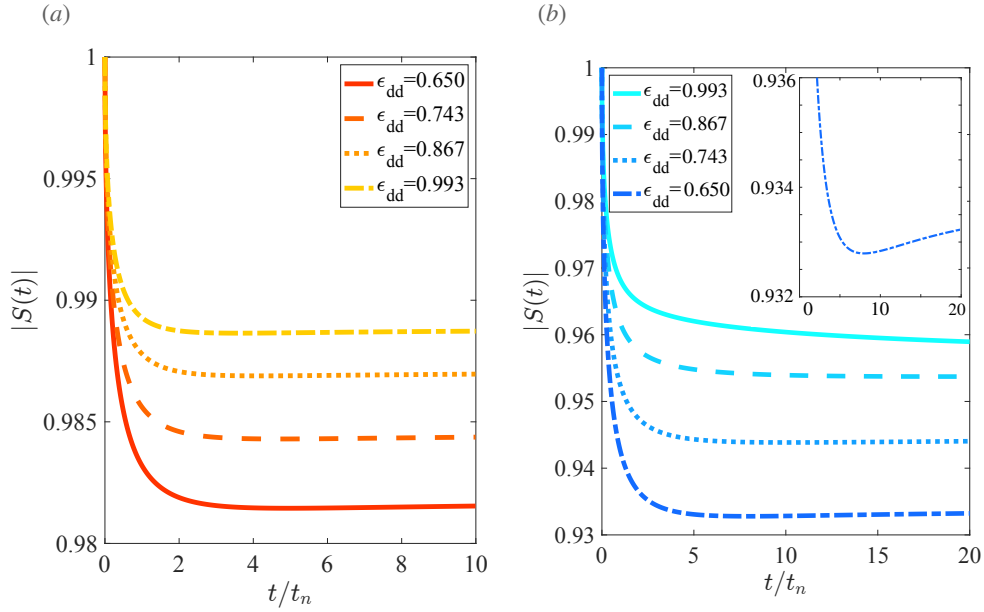


Figure 3: **Amplitude of the contrast** (a) Amplitude as a function of time for $a_{12} = a_{11}$ and different values of ϵ_{dd} . (b) Amplitude as a function of time for $a_{12} = 2a_{11}$. In both plots, we fix the dipolar coupling strengths as $d_2 = d_1 = 130.04a_0$. (Inset) Slowdown of the dynamics due to a rich dipolar character of the bath.

4.4 Anisotropy of time evolution

Up to now, we have considered quantities integrated over all directions, which cannot show the anisotropy of the time evolution. However, in general, the impurity experiences direction-dependent dynamics, with the limiting cases given when its momentum is parallel or perpendicular to the dipole direction; following Ref. [31] we call these the axial and radial cases, respectively. When $\epsilon_{dd} \neq 0$, the energy cost to create a phonon with $\theta = 0$ is higher than the energy cost to create a phonon with $\theta = \pi/2$, see Fig. 1 (a). Therefore, we expect that the movement of the impurity is affected more strongly in the radial direction (unless V_{12} is also vanishing in this direction), which is further reflected in the values of the radial and axial effective masses in the steady state, see App. B. The latter effective mass is always weakly renormalized, while the former increases rapidly, implying slow diffusion in the radial direction.

To quantify the discussion above, and to illustrate the slowing-down of the radial dynamics compared to the axial dynamics, we study the number of excitations as a function of the angle: $B(\theta) = \sum_{\mathbf{k}'} |\beta_{\mathbf{k}'}|^2 \delta(\cos(\theta) - \cos(\theta'))$ where $\mathbf{k}' = \{k', \theta', \phi'\}$ is the integration index:

$$B_\theta(t) = \sqrt{\frac{16na_{11}^3}{\pi}} \left(\frac{a_{12}}{a_{11}}\right)^2 \int dx \frac{xz(u)^2 \left[1 - \cos\left(x^2 \frac{t}{t_n} + x \frac{t}{t_n} \sqrt{x^2 + w(u)}\right)\right]}{(x + \sqrt{x^2 + w(u)})^2 \sqrt{x^2 + w(u)}}. \quad (9)$$

This function features different time scales for different angles, see Fig. 1 (b), demonstrating that the time evolution of the dipolar polaron is drastically different from what is expected for short-range interactions. Physical insight into the anisotropy can be gained by considering the short-time dynamics, i.e., $t \ll t_n$. In this limit, we derive $B(\theta) \simeq \sqrt{t/t_F^\theta}$, where

$$t_F^\theta = \frac{m}{32\pi n^2 [a_{12} + \sqrt{d_1 d_2} (3 \cos^2(\theta) - 1)]^4}. \quad (10)$$

The timescale t_F^θ depends on the angle, showing the difference in the dynamics parallel and perpendicular to the dipolar moment. One striking example is the dynamics with $a_{12} = \sqrt{d_1 d_2}$,

which leads to weak interactions for $\theta = \pi/2$ and consequently $t_F^{\theta \rightarrow \pi/2} \rightarrow \infty$ [cf. the bottom panel of Fig. 1 (b)].

Note that the anisotropy of t_F^θ is due to the dipolar nature of the impurity, and vanishes if we assume that $d_2 = 0$ [cf. the top panel of Fig. 1 (b)]. For longer times, the anisotropy of the dynamics is also driven by the anisotropy of the medium. It exists even if $d_2 = 0$, provided that $d_1 \neq 0$. This can be shown using $\beta_{\mathbf{k}}$ from the saddle point approximation. The existence of the anisotropy for $d_2 = 0$ can be also anticipated from the directional dependence of the effective mass, see App. B.

Finally, we mention another manifestation of anisotropy of time evolution which can be observed when the velocity of the impurity is close to the speed of sound. In this case, there is a ‘‘slowdown’’ dynamics [24]. In the non-dipolar case, the impurity exhibits a critical slowdown near the critical momentum $p_c = mc_0$. However, in the dipolar case, the slowdown appears when the impurity momentum resonates with a specific sound mode in a particular direction, namely the impurity will experience the slowdown more readily in the radial direction – the effect will be particularly strong if ϵ_{dd} is close to one.

4.5 Trapped system

Many properties of dipolar impurities in the homogeneous system can be understood at the qualitative level from the case with zero-range interactions by simply assuming that the s -wave scattering length depends on the direction. The physics of the problem becomes more intricate in the presence of inhomogeneous trapping, due a possible interplay between the trap geometry and the anisotropy of the interaction. To illustrate this, we use the local-density approximation to study the experimentally relevant case of a system in a harmonic trap, see, e.g., [36]. We assume that the dipolar condensate is confined by the external potential $V(\rho, z) = \frac{1}{2}m\omega_z^2(\lambda^2\rho^2 + z^2)$, with dipoles pointing along the z -direction, $\lambda = \omega_\rho/\omega_z$, and study the role of different geometries on the dynamics of the contrast. For simplicity, we assume that the impurity does not experience any external potential.

In Fig. 4 (a) we present the amplitude and the phase of the contrast averaged over the Bose gas confined by a cigar-shaped ($\lambda = 0.1$), and a spherical ($\lambda = 1$) traps, which correspond to $(\omega_\rho, \omega_z) = 2\pi(50, 500)\text{Hz}$ and $(\omega_\rho, \omega_z) = 2\pi(500, 500)\text{Hz}$, respectively. To calculate the contrast, we rely on the local-density approximation ($n \rightarrow n(\mathbf{r})$):

$$S = \frac{1}{N} \int d^3\mathbf{r} n(\mathbf{r}) \exp \left[-\frac{i\mathcal{E}(\mathbf{r})t}{\hbar} + \frac{4i}{3} \sqrt{\frac{n(\mathbf{r})a_{11}^3}{\pi}} \left(\frac{a_{12}}{a_{11}} \right)^2 \mathcal{R} \left(\frac{8\pi\hbar a_{11} n(\mathbf{r})t}{m} \right) \right], \quad (11)$$

where $\mathcal{E}(\mathbf{r}) = \int d^3\mathbf{r}' V_{12}(\mathbf{r} - \mathbf{r}')n(\mathbf{r}') + \gamma(\mathbf{r}) \int du z(u)^2 w(u)^{1/2}$. Note that we use the real-space representation of V_{12} only at the mean-field level in \mathcal{E} . This allows us to account for the leading-order effect of the long-range tail of dipole-dipole interactions. The bosonic density for our system with $N = 2 \times 10^4$ atoms is conveniently calculated using the Gaussian variational ansatz [43]

$$n(\rho, z) = \frac{N}{\pi^{3/2} l_\rho^2 l_z a_H^3} \exp \left[-\frac{1}{a_H^2} \left(\frac{\rho^2}{l_\rho^2} + \frac{z^2}{l_z^2} \right) \right], \quad (12)$$

where l_ρ and l_z are variational parameters found by minimizing the energy; $a_H = \sqrt{\hbar/m\bar{\omega}}$ is the harmonic oscillator length with $\bar{\omega} = (\omega_\rho^2\omega_z)^{1/3}$. The Bose gas in a trap will have an anisotropic density, which plays an important role in time evolution, as can be seen by comparing the left and the right panels in Fig. 4(a).

The short-time dynamics of the contrast can be computed using Eq. (5)

$$S(t) \approx 1 - (1-i)\beta \sqrt{\frac{t}{t_n^0}} - \frac{i}{4\sqrt{2}} \left[\frac{a_{12}}{a_{11}} + \frac{\sqrt{d_1 d_2}}{a_{11}} \kappa(\Delta^{-1}) \right] \frac{t}{t_n^0}, \quad (13)$$

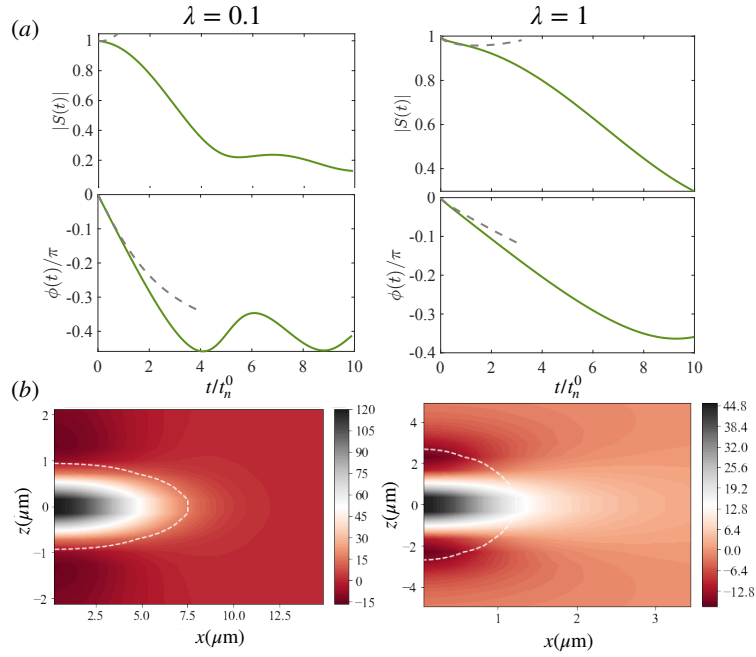


Figure 4: **Dynamics in a trap** (a) Contrast (amplitude and phase) as a function of time for an oblate trap $(\omega_\rho, \omega_z) = 2\pi(50, 500)$ (green solid), and for a spherical trap $(\omega_\rho, \omega_z) = 2\pi(500, 500)$ (grey dashed). Here, $\epsilon_{dd} \sim 1$ and $a_{12} = a_{11}$. (b) Steady-state local polaron energy (at the mean-field level) $E_0(\mathbf{r}) = \int d^3\mathbf{r}' V_{12}(\mathbf{r} - \mathbf{r}')n(\mathbf{r}')$ for the two aforementioned cases. To illustrate the shape of the condensate, we draw (dashed curve) a contour of the condensate when its density is at a 10% of the peak value.

where $\beta = \sqrt{\frac{1}{2}n_0 a_{11}^3 \left(\frac{a_{12}^2 + \frac{4}{5}d_1 d_2}{a_{11}^2} \right)}$ and the timescale depends on the peak density, $n_0 = n(0)$, $t_n^0 = \frac{m}{8\pi\hbar n_0 a_{11}}$. The function κ is defined as (cf. [43]) $\kappa(\Delta^{-1}) = \frac{(1+2\Delta^2)}{(\Delta^2-1)} - \frac{3\Delta^2 \arctan \sqrt{\Delta^2-1}}{(\Delta^2-1)^{3/2}}$ with $\Delta = l_z/l_\rho$. The last term in Eq. (13) originates from the local polaron energy at the level of first order perturbation theory (see App. D for more details). The interplay between the dipole-dipole interaction and the geometry of the potential enters Eq. (13) via the term $\sqrt{d_1 d_2} \kappa$. By changing the shape of the trap one varies κ in the range $[-1, 2]$, and consequently the energy exchange between the impurity and the bath, see Fig. 4, which illustrates distinctly different approach to steady states for the two values of λ . Note that in the limiting case $a_{12} = -\sqrt{d_1 d_2} \kappa(l_\rho/l_z)$, the average polaron energy at the mean-field level vanishes, slowing down the dynamics. This regime amplifies the importance of the \sqrt{t} term and beyond-mean-field effects (see Eq. (13)) in a dipolar mixture, suggesting the contrast as a probe of novel physics.

The local-density approximation utilized above is accurate only if the impurity can explore a small region of space. This assumption is adequate for studies of time evolution on timescales given by $t_n \sim 0.1\text{ms}$ (compare with timescales for the dynamics in the trap $2\pi/\bar{\omega} \simeq 2\text{ms}$). Time evolution of the impurity cloud at longer times deserves a further investigation. To motivate it, we present in Fig. 4(b) the local polaron energy $E_0(\mathbf{r})$ (see App. D) for the previously considered scenarios with $\lambda = 0.1$ and $\lambda = 1$. We see that in the former case the energy of the impurity is minimized when it is expelled from the condensate. In contrast, in the latter case, the impurity prefers to localize outside the condensate along the z -axis (cf. Ref. [49]).

4.6 Outlook

In this work the host medium is a Bose-Einstein condensate, however, our results can be easily extrapolated to impurities immersed in an isolated droplet or in a dipolar supersolid. A possible interesting future direction is to study the polaron dynamics across the superfluid-to-supersolid transition using dipolar or non-dipolar impurities embedded in dipolar media [50, 51]. This transition is expected to have an unusual phase diagram [52], and the impurity dynamics may provide a tool to probe it.

Another direction is to consider multiple dipolar polarons and their interactions induced by the medium. In contrast to systems with short-range interactions [53–55], the anisotropic nature of the dipole-dipole potential will induce anisotropic correlations between impurities. These can be observed experimentally for example by studying the anisotropy of the impurity cloud in quench dynamics (cf. Ref. [56]).

Dipolar polarons in quantum gases may provide a valuable insight into out-of-equilibrium dynamics of indirect excitons modelled as electric dipoles. Interaction and trapping in these solid-state systems can be controlled, making it possible to study out-of-equilibrium dipolar excitons in atomically thin semiconductors [57]. These systems garner significant attention due to their unique optical properties, and their quantum simulation may not only deepen our understanding of dipolar excitations, but also lead to novel technological applications.

Acknowledgements

We thank Lauriane Chomaz for useful discussions and comments on the manuscript. We also thank Ragheed Al Hyder for comments on the manuscript.

Author contributions The project was conceived by L.A.P.A. All authors contributed to the analysis of numerical data, and to the development of the manuscript. A.G.V, G.B. and L.A.P.A. contributed equally to this work.

Funding information G.B. acknowledges support from the Austrian Science Fund (FWF), under Project No. M2641-N27. This work is supported by the Deutsche Forschungsgemeinschaft (DFG, German Research Foundation) under Germany’s Excellence Strategy EXC2181/1-390900948 (the Heidelberg STRUCTURES Excellence Cluster). A. G. V. acknowledges support from the European Union’s Horizon 2020 research and innovation programme under the Marie Skłodowska-Curie Grant Agreement No. 754411. L.A.P.A acknowledges by the PNRR MUR project PE0000023 - NQSTI and the Deutsche Forschungsgemeinschaft (DFG, German Research Foundation) under Germany’s Excellence Strategy - EXC - 2123 Quantum Frontiers-390837967 and FOR2247.

A On the accuracy of the Fröhlich Hamiltonian

To investigate the effects of beyond-Fröhlich physics, let us consider the terms that describe other relevant scattering processes such as

$$\mathcal{H}_{\text{BF}} = \frac{1}{V} \sum_{\mathbf{k}, \mathbf{q}} V_{\mathbf{k}\mathbf{q}}^{(1)} e^{i(\mathbf{k}-\mathbf{q}) \cdot \hat{\mathbf{r}}} \hat{b}_{\mathbf{k}}^\dagger \hat{b}_{\mathbf{q}} + \frac{1}{V} \sum_{\mathbf{k}, \mathbf{q}} V_{\mathbf{k}\mathbf{q}}^{(2)} e^{i(\mathbf{k}+\mathbf{q}) \cdot \hat{\mathbf{r}}} \left(\hat{b}_{\mathbf{k}}^\dagger \hat{b}_{\mathbf{q}}^\dagger + \hat{b}_{-\mathbf{k}} \hat{b}_{-\mathbf{q}} \right), \quad (\text{S1})$$

where

$$V_{\mathbf{k}\mathbf{k}'}^{(1,2)} = \frac{1}{2} V_{12}(\mathbf{k}' \mp \mathbf{k}) \left[W_{\mathbf{k}} W_{\mathbf{k}'} \pm \frac{1}{W_{\mathbf{k}} W_{\mathbf{k}'}} \right]. \quad (\text{S2})$$

The upper (lower) sign corresponds to $V_{\mathbf{k}\mathbf{k}'}^{(1)}$ ($V_{\mathbf{k}\mathbf{k}'}^{(2)}$). This Hamiltonian leads to the following equations for the parameters $\beta_{\mathbf{k}}$, which appear in our variational ansatz,

$$i\hbar\dot{\beta}_{\mathbf{k}} = \frac{\sqrt{n}}{\sqrt{V}}V_{12}(\mathbf{k})W_{\mathbf{k}} + \Omega_{\mathbf{k}}\beta_{\mathbf{k}} + \frac{1}{V}\sum_{\mathbf{k}'}V_{\mathbf{k}\mathbf{k}'}^{(1)}\beta_{\mathbf{k}'} + \frac{1}{V}\sum_{\mathbf{k}'}V_{\mathbf{k}\mathbf{k}'}^{(2)}\beta_{\mathbf{k}'}^*. \quad (\text{S3})$$

The equation for $\phi(t)$ remain unchanged.

The last two terms in Eq. (S3) describe the beyond-Fröhlich-Hamiltonian physics. Note that their effect is next-to-leading order (in powers of V_{12}) because the source term, $\sqrt{n}V_{12}(\mathbf{k})W_{\mathbf{k}}/\sqrt{V}$, for $\beta_{\mathbf{k}}$ is proportional to $\sqrt{n}V_{12}$, which is a small parameter for experimentally relevant densities. Therefore, these terms can be neglected in our work (at least within our variational approach), as the properties that we calculate are determined by $|\beta_{\mathbf{k}}|^2$. Note that the beyond-Fröhlich terms are important for the case $|a_{ij}| \gg d_i$, which can be described using the framework developed to study non-dipolar polarons.

B Static properties of the system

Below, we provide three appendices with technical details that support results presented in the main text. In App. B, we compute the polaron properties, including its energy, quasiparticle residue, and effective mass. The energy will later enter as an input in the calculation of the contrast. The energy is computed using second-order perturbation theory with either the bare impurity-boson perturbing potential or the renormalized one derived by excluding high-energy momentum states. In App. C, we derive the analytical expression for the contrast, see Eq. (4) of the main text. In App. D, we use a Gaussian density profile to compute the energy in a trapped case, which allows us to highlight the underlying effects in polaron's anisotropy dynamics

1. Lee-Low-Pines transformation (LLPt). In impurity problems, a transformation to the co-moving frame of the impurity is customary and simplifies the calculations. We transform the Hamiltonian, $\mathcal{H}' \rightarrow \hat{S}^{-1}\mathcal{H}\hat{S}$, by means of the operator $\hat{S} = \exp(i\hat{\mathbf{r}} \cdot \hat{\mathbf{P}}_{\text{B}})$ where $\hat{\mathbf{P}}_{\text{B}} = \hbar\sum_{\mathbf{k}}\mathbf{k}\hat{b}_{\mathbf{k}}^{\dagger}\hat{b}_{\mathbf{k}}$ is the total momentum of bosons. At the Fröhlich level, we derive

$$\hat{S}^{-1}\mathcal{H}\hat{S} = \frac{(\hat{\mathbf{P}} - \hat{\mathbf{P}}_{\text{B}})^2}{2} + \sum_{\mathbf{k}}\omega_{\mathbf{k}}\hat{b}_{\mathbf{k}}^{\dagger}\hat{b}_{\mathbf{k}} + nV_{12}(\mathbf{k}=0) + \frac{\sqrt{n}}{\sqrt{V}}\sum_{\mathbf{k}\neq 0}V_{12}(\mathbf{k})W_{\mathbf{k}}(\hat{b}_{\mathbf{k}} + \hat{b}_{-\mathbf{k}}^{\dagger}). \quad (\text{S4})$$

Note that the total momentum $\hat{\mathbf{P}}$ can be considered constant here.

2. Ground-state energy. The polaron energy is among the key quantities that describe static and dynamic properties of the system, in particular, the contrast. To use methods of many-body perturbation theory, we write the Hamiltonian Eq. (S4) as

$$\begin{aligned} \mathcal{H} &= \mathcal{H}_0 + \mathcal{H}_{int}, \\ \mathcal{H}_0 &= \frac{(\mathbf{P} - \hat{\mathbf{P}}_{\text{B}})^2}{2} + \sum_{\mathbf{k}}\omega_{\mathbf{k}}\hat{b}_{\mathbf{k}}^{\dagger}\hat{b}_{\mathbf{k}}, \\ \mathcal{H}_{int} &= nV_{12}(\mathbf{k}=0) + \frac{\sqrt{n}}{\sqrt{V}}\sum_{\mathbf{k}\neq 0}V_{12}(\mathbf{k})W_{\mathbf{k}}(\hat{b}_{\mathbf{k}} + \hat{b}_{-\mathbf{k}}^{\dagger}), \end{aligned} \quad (\text{S5})$$

where \mathbf{P} is a complex number – the total momentum of the system. The first-order correction in perturbation theory is trivial for the homogeneous case $E_0^{(1)} = \langle 0 | \mathcal{H}_{int} | 0 \rangle$ where $|0\rangle$ is the state

consisting of a single impurity with momentum \mathbf{P} and the vacuum of phonons. The second-order correction reads

$$E_0^{(2)} = \sum_{\mathbf{k} \neq 0} \frac{|\langle \mathbf{k} | \mathcal{H}_{int} | 0 \rangle|^2}{E_0^{(0)} - E_{\mathbf{k}}^{(0)}} = -\frac{n}{V} \sum_{\mathbf{k}} \frac{|g_{12} + g_{12}^{(d)} (3 \cos^2 \theta_k - 1)|^2 W_{\mathbf{k}}^2}{\Omega_{\mathbf{k}}(\mathbf{P})}, \quad (\text{S6})$$

where $\Omega_{\mathbf{k}}(\mathbf{P} \rightarrow 0) \approx (\epsilon_{\mathbf{k}} + \omega_{\mathbf{k}})$ for slow impurities. Using the definition of the contact g_{ij} and dipolar coupling strengths $g_{ij}^{(d)}$ defined in the main text, we re-write this expression as

$$E_0^{(2)} = -\frac{32}{\sqrt{\pi}} (na_{11}^3)^{3/2} \frac{\hbar^2}{ma_{11}^2} \left(\frac{a_{12}}{a_{11}} \right)^2 \int_{-1}^1 \int_0^\infty dudx \frac{x^2 z(u)^2}{\sqrt{x^2 + w(u)} (x + \sqrt{x^2 + w(u)})}. \quad (\text{S7})$$

where $x = k\xi/\sqrt{2}$, $\xi = \hbar/\sqrt{2mg_{11}n}$ and $u = \cos \theta_k$. We have defined the auxiliary functions:

$$\begin{bmatrix} w(u) \\ z(u) \end{bmatrix} = \begin{bmatrix} 1 + \epsilon_{dd} (3u^2 - 1) \\ 1 + \bar{\epsilon}_{dd} (3u^2 - 1) \end{bmatrix} \quad (\text{S8})$$

with $\epsilon_{dd} = d_1/a_{11}$ and $\bar{\epsilon}_{dd} = \sqrt{d_1 d_2}/a_{12}$. The integral in Eq. (S7) diverges and should be regularized. Similar to the contact case, we do so by disregarding the short-wavelength phonons which are irrelevant in the polaron physics. To this end, we note that the integral

$$\lim_{x \rightarrow \infty} \int_{-1}^1 \int_0^\infty dudx \frac{x^2 z(u)^2}{\sqrt{x^2 + w(u)} (x + \sqrt{x^2 + w(u)})} = \frac{1}{2} \int du z(u)^2. \quad (\text{S9})$$

should be removed from Eq. (S7), which leads to

$$E_0^{(2)} = 32\sqrt{\pi} (na_{11}^3)^{3/2} \frac{\hbar^2}{ma_{11}^2} \left(\frac{a_{12}}{a_{11}} \right)^2 \int_{-1}^1 dudx \left\{ \frac{z(u)^2}{2} - \frac{x^2 z(u)^2}{\sqrt{x^2 + w(u)} (x + \sqrt{x^2 + w(u)})} \right\}. \quad (\text{S10})$$

This expression is further simplified

$$E_0^{(2)} = \frac{128\sqrt{\pi}}{3} (na_{11}^3)^{3/2} \frac{\hbar^2}{ma_{11}^2} \left(\frac{a_{12}}{a_{11}} \right)^2 \int_0^1 du z(u)^2 \sqrt{w(u)}, \quad (\text{S11})$$

which coincides with the expression obtained with the Hugenholtz-Pines formalism in [49].

3. Regularized potential. In the previous section, we computed the polaron energy using bare potentials. Alternatively, we could have used a regularized potential for these calculations. To find forms of the regularized potentials, we note that a dipolar Bose gas within a mean-field approximation can be described with the potential from the first Born approximation, see, e.g., [58–60]. Therefore, as long as we focus on a weakly-interacting Bose gas, our expression for V_{11} is accurate. For any beyond mean-field calculations, this potential clearly fails, as can be seen by solving a few-body problem already with $g_{ij}^d = 0$, see, e.g., [61]. Therefore, we need to suggest an effective description for V_{12} . For our purposes, the effective interaction follows from the first and second terms in Born approximation. Using $V_{12} = \frac{4\pi\hbar^2}{m} (a_{12} + \sqrt{d_1 d_2} (3 \cos^2 \theta_k - 1))$ and

$$V_{12}^{(\Lambda)} = \frac{4\pi\hbar^2}{m} \left(a_{12} + \sqrt{d_1 d_2} \frac{8}{5\pi} \Lambda + \frac{2a_{12}^2}{\pi} \Lambda \right), \quad (\text{S12})$$

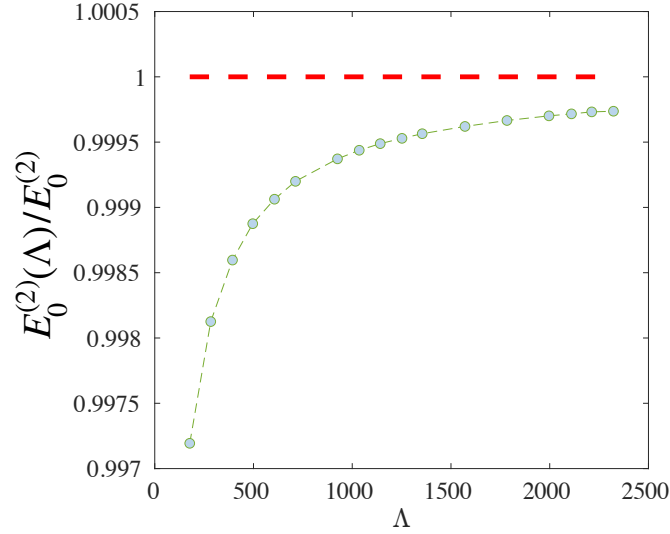


Figure S1: Beyond mean-field energy $E_0^{(2)}(\Lambda)/E_0^{(2)}$ computed with the exact Hugenholtz-Pines (HP) (red dashed line) formalism and the regularized correction (green points) as a function of the cut-off Λ (in the units given by $n^{1/3}$). We find that $E_0^{(2)}(\Lambda) = E_{\text{HP}}^{(2)} + \frac{\alpha}{\beta - \Lambda}$, confirming our regularization procedure. Here $a_{12} = 150a_0$.

where Λ is the high-momentum cut-off parameter, we compute the polaron energy

$$E_0 = V_{12}^\Lambda n + \frac{\mathbf{P}^2}{2m} - \frac{n}{V} \sum_{\mathbf{k}} \frac{V_{12}^2(\mathbf{k}) W_{\mathbf{k}}^2}{\omega_{\mathbf{k}} + \frac{\hbar^2 \mathbf{k}^2}{2m} - \frac{\hbar \mathbf{k} \cdot \mathbf{P}}{m}}. \quad (\text{S13})$$

In the thermodynamic limit $\sum_{\mathbf{k}} \rightarrow V/(2\pi)^3 \int d^3\mathbf{k}$ and $\mathbf{P} = 0$, this expression reads

$$E_0 = V_{12}^\Lambda n - \int_0^{\frac{\Lambda}{n^{1/3}}} dk \int_{-1}^1 dx \frac{8\hbar^2 k^2 n^{4/3} [a_{12} + \sqrt{d_1 d_2} (3x^2 - 1)]^2}{m \sqrt{k^2 + 16\pi(a_{11} + d_1(3x^2 - 1))n^{1/3}} (k + \sqrt{k^2 + 16\pi(a_{11} + d_1(3x^2 - 1))n^{1/3}})}.$$

It is straightforward to show that it coincides with the result within the Hugenholtz-Pines formalism (see Eq. (S11)) for Λ . To this end, use the integral

$$\int_0^\infty dp \left(\frac{p^2}{\sqrt{p^2 + F}(p + \sqrt{p^2 + F})} - \frac{1}{2} \right) = -\frac{2\sqrt{F}}{3}, \quad (\text{S14})$$

where F is some constant. In Fig. S1 we compare the polaron energy using from the Hugenholtz-Pines against the energy based upon the regularized potential.

The equations for β and ϕ , regularized in the second-order in the impurity-boson interaction strength, read as follows

$$i\hbar \dot{\beta}_{\mathbf{k}} = \frac{\sqrt{n}}{\sqrt{V}} V_{12}(\mathbf{k}) W_{\mathbf{k}} + \Omega_{\mathbf{k}} \beta_{\mathbf{k}}, \quad (\text{S15})$$

$$\dot{\phi} = V_{12}^\Lambda n + \frac{\mathbf{P}^2 - \mathbf{P}_{\text{B}}^2}{2m} + \frac{\sqrt{n}}{\sqrt{V}} \sum_{\mathbf{k}} W_{\mathbf{k}} V_{12}(\mathbf{k}) \Re \epsilon[\beta_{\mathbf{k}}]. \quad (\text{S16})$$

Note that V_{12}^Λ is used only in the equation for $\dot{\phi}$. This is expected – recall that the parameter $\beta_{\mathbf{k}}$ is proportional to V_{12} .

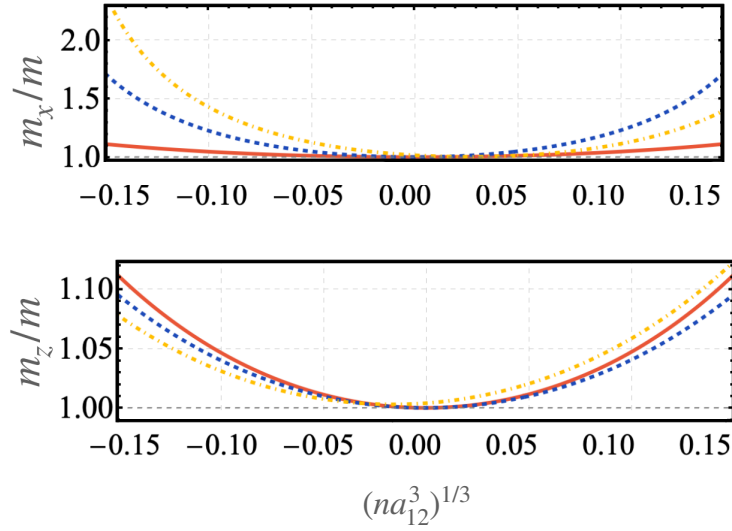


Figure S2: (Top) The effective mass along the x axis, m_x , as a function of the (dimensionless) interspecies scattering length a_{12} , assuming that $a_{11} = 130.041a_0$. The different curves take into account different regimes. The solid curve is for a system with only contact interactions, i.e., $d_1 = d_2 = 0$; the dashed curve illustrates the case with $d_2 = 0$; the dashed-dotted curve shows the mass for a dipolar impurity in a dipolar medium, see the text for details. (Bottom) The effective mass along the z axis m_z , as a function of the (dimensionless) interspecies scattering length a_{12} . The different curves take into account different regimes, see the text for details. Notice the different scaling of the y -axis in comparison to the upper panel.

4. Quasiparticle residue. At the level of second-order perturbation theory, the residue is

$$Z = 1 - \frac{1}{V} \sum_{\mathbf{k}} \frac{|\langle \mathbf{k} | \mathcal{H}_{int} | 0 \rangle|^2}{(E_0^{(0)} - E_{\mathbf{k}}^{(0)})^2}, \quad (\text{S17})$$

which leads to

$$Z = 1 - \frac{8}{3\sqrt{\pi}} \left(\frac{a_{12}}{a_{11}} \right)^2 \sqrt{na_{11}^3} \int_0^1 du \frac{z(u)^2}{w(u)^{1/2}}, \quad (\text{S18})$$

where (as before) $x = k\xi/\sqrt{2}$ and $u = \cos \theta_{\mathbf{k}}$. Note that this expression coincides with the first two terms of Taylor series of Eq. (7) of the main text, providing another validation of the variational ansatz.

5. Effective mass. The polaron energy as a function of \mathbf{P} (see Eq. (S13)) allows us to compute the effective masses of the polaron, m_x , m_y and m_z , defined from

$$E_0(P) = E_0(\mathbf{P} = \mathbf{0}) + \frac{P_x^2}{2m_x} + \frac{P_y^2}{2m_y} + \frac{P_z^2}{2m_z}. \quad (\text{S19})$$

Assuming that the momentum of the impurity is much smaller than the speed of sound (in all directions), we derive

$$\frac{m}{m_{i=x,y,z}} = 1 - \frac{2\hbar^2 n}{Vm} \sum_{\mathbf{k}} \frac{[V_{12}(\mathbf{k})W_{\mathbf{k}}]^2 k_i^2}{\left(\omega_{\mathbf{k}} + \frac{\hbar^2 k^2}{2m}\right)^3}, \quad (\text{S20})$$

where (as in the main text) $m = m_2 = m_1$. Due to the axial symmetry of the problem, the directions x and y are identical, and therefore, we can focus only on the effective masses in x and z directions. These masses in the thermodynamic limit are

$$\frac{m}{m_x} = 1 - \frac{\hbar^2 n}{4\pi^3 m} \int d\mathbf{k} \frac{[V_{12}(\mathbf{k})W_{\mathbf{k}}]^2 k_x^2}{\left(\omega_{\mathbf{k}} + \frac{\hbar^2 k^2}{2m}\right)^3}, \quad \frac{m}{m_z} = 1 - \frac{\hbar^2 n}{4\pi^3 m} \int d\mathbf{k} \frac{[V_{12}(\mathbf{k})W_{\mathbf{k}}]^2 k_z^2}{\left(\omega_{\mathbf{k}} + \frac{\hbar^2 k^2}{2m}\right)^3}. \quad (\text{S21})$$

Using the definitions from above, these expressions can be further simplified as

$$\left(\frac{m/m_x}{m/m_z} \right) = 1 - \frac{8\sqrt{na_{11}^3}}{\sqrt{\pi}} \left(\frac{a_{12}}{a_{11}} \right)^2 \int dx du \frac{x^2 z(u)^2}{\sqrt{x^2 + w(u)}(x + \sqrt{x^2 + w(u)})^3} \begin{pmatrix} 1 - u^2 \\ 2u^2 \end{pmatrix}.$$

In the limit of $d_2 \rightarrow 0$ (non-dipolar) impurity these expressions reproduce the results presented in [31], providing us with another validation of our variational approach.

We note that the effective masses m_x and m_z are identical if the medium is isotropic, i.e., $m_x = m_z$ if $d_1 = 0$. The difference between m_x and m_z persists even for a non-dipolar impurity $d_2 \rightarrow 0$ ($a_{12}/d_2 \gg 1$) if $d_1 \neq 0$ (see also Ref. [31]). If $\sqrt{d_1 d_2} \simeq a_{12}$ the effective masses are affected by the dipole moments of the impurity and bosons.

To illustrate this, we calculate the effective masses for Dysprosium atoms assuming $a_{11} = 130.041a_0$ and $n = 10^{20}m^{-3}$. The value of a_{11} is chosen such that the system is stable, i.e., V_{11} is always positive. In Fig. S2, we show the effective masses for (i) the contact case ($d_1 = d_2 = 0$); (ii) a dipolar medium with a contact impurity ($d_2 = 0, d_1 = 130a_0$); (iii) a dipolar medium with a dipolar impurity ($d_1 = d_2 = 130a_0$). We see that the mass m_z is only weakly affected by the dipolar nature of the interaction, whereas m_x is strongly modified, which may be observed by means of momentum-resolved Bragg spectroscopy. The effective mass anisotropy that we report is accessible within current experimental resolutions.

Finally, let us discuss what happens in the limit $\epsilon_{dd} \rightarrow 0$, i.e., in the vicinity of the collapse of the Bose gas. The effective mass m_z stays finite even if $\epsilon_{dd} = 1$. The mass m_x however diverges. One can show that $m/m_x - 1 \sim \ln(1 - \epsilon_{dd})$.

C Derivation of contrast

Here, we outline the most important steps in the derivation of Eq. (4) of the main text. Starting from Eq. (2), we write $\phi(t)$ as

$$\phi(t) = \frac{1}{\hbar} \int_0^t ds \left[V_{12}(\mathbf{k})n + \frac{\sqrt{n}}{2\sqrt{V}} \sum_{\mathbf{k}} V_{12}(\mathbf{k})W_{\mathbf{k}} (\beta_{\mathbf{k}}(s) + \beta_{\mathbf{k}}^*(s)) \right], \quad (\text{S22})$$

where the explicit solution of $\beta_{\mathbf{k}}(t)$ is $\beta_{\mathbf{k}}(t) = V_{12}(\mathbf{k}) \frac{\sqrt{n}}{\sqrt{V}} \frac{W_{\mathbf{k}}}{\Omega_{\mathbf{k}}} \left[\exp\left(\frac{i\Omega_{\mathbf{k}}t}{\hbar}\right) - 1 \right]$, which leads to

$$\phi(t) = \frac{1}{\hbar} \int_0^t ds \left\{ V_{12}(\mathbf{k})n + \frac{n}{V} \sum_{\mathbf{k}} \frac{V_{12}(\mathbf{k})^2 W_{\mathbf{k}}^2}{\Omega_{\mathbf{k}}} [\cos(\Omega_{\mathbf{k}}t/\hbar) - 1] \right\}. \quad (\text{S23})$$

It is convenient to split this integral into two parts with time-dependent and time-independent integrands:

$$\phi(t) = \overbrace{\int_0^t \frac{ds}{\hbar} \left\{ V_{12}(\mathbf{k})n - \frac{n}{V} \sum_{\mathbf{k}} \frac{V_{12}(\mathbf{k})^2 W_{\mathbf{k}}^2}{\Omega_{\mathbf{k}}} \right\}}^{I_1(t)} + \overbrace{\int_0^t \frac{ds}{\hbar} \left\{ \frac{n}{V} \sum_{\mathbf{k}} \frac{V_{12}(\mathbf{k})^2 W_{\mathbf{k}}^2}{\Omega_{\mathbf{k}}} \cos(\Omega_{\mathbf{k}}s/\hbar) \right\}}^{I_2(t)}.$$

The integral $I_1(t)$ is identical to the one appearing in our calculations of the polaron energy (see Sec. B), namely $I_1(t) = E_0 t / \hbar$. Note that regularization of the potential is taken into account here. The second integral $I_2(t)$ can be written as

$$I_2(t) = \frac{1}{\hbar} \int_0^t ds \left\{ \frac{n}{V} \sum_{\mathbf{k}} \frac{V_{12}(\mathbf{k})^2 W_{\mathbf{k}}^2}{\Omega_{\mathbf{k}}} \cos(\Omega_{\mathbf{k}} s / \hbar) \right\} = \frac{n}{V} \sum_{\mathbf{k}} \frac{V_{12}(\mathbf{k})^2 W_{\mathbf{k}}^2}{\Omega_{\mathbf{k}}^2} \sin(\Omega_{\mathbf{k}} t / \hbar),$$

so that

$$\phi(t) = I_1(t) + I_2(t) = Et / \hbar + \frac{n}{V} \sum_{\mathbf{k}} \frac{V_{12}(\mathbf{k})^2 W_{\mathbf{k}}^2}{\Omega_{\mathbf{k}}^2} \sin(\Omega_{\mathbf{k}} t / \hbar) \quad (\text{S24})$$

For the contrast, we also need to calculate the expression

$$\sum_{\mathbf{k}} |\beta_{\mathbf{k}}(t)|^2 = \frac{2n}{V} \sum_{\mathbf{k}} \frac{V_{12}(\mathbf{k})^2 W_{\mathbf{k}}^2}{\Omega_{\mathbf{k}}^2} [1 - \cos(\Omega_{\mathbf{k}} t / \hbar)]. \quad (\text{S25})$$

Using ϕ and β in the definition of the contrast, $S(t) = \exp \left[-i\phi(t) + \frac{1}{2} \sum_{\mathbf{k}} |\beta_{\mathbf{k}}(t)|^2 \right]$, we derive

$$S(t) = \exp \left[-i\bar{E}\bar{t} - \frac{4}{\sqrt{\pi}} \sqrt{na_{11}^3} \left(\frac{a_{12}}{a_{11}} \right)^2 \int dudx \frac{x^3 z(u)^2}{\sqrt{x^2 + w\bar{\Omega}_x^2}} \left(e^{-i\bar{\Omega}_x \bar{t}} - 1 \right) \right], \quad (\text{S26})$$

where we use dimensionless variables, $\bar{\Omega}_x = (x^2 + x\sqrt{x^2 + w})$; $\bar{t} = t/t_n$ with $t_n = \frac{m}{8\pi\hbar na_{11}}$. The auxiliary functions $z(u)$ and $w(u)$ are defined in Eq. (S8). The integrand appearing in Eq. (S26) can be written as a primitive function and simplified further by using the procedure outlined in Appendix D of Ref. [24]. The primitive reads

$$K = -i \int du z(u)^2 \int dx \int_0^{\bar{t}} ds \frac{x^3}{\sqrt{x^2 + w(u)\bar{\Omega}_x}} e^{-i\bar{\Omega}_x s}. \quad (\text{S27})$$

Using $x = \bar{\Omega}_x / \sqrt{w(u) + 2\bar{\Omega}_x}$, $dx = (\bar{\Omega}_x + w)(w + 2\bar{\Omega}_x)^{-3/2} d\bar{\Omega}_x$ and $\sqrt{x^2 + w} = (\bar{\Omega}_x + w)(w + 2\bar{\Omega}_x)^{-1/2}$, the function K is further simplified:

$$K = \int du z(u)^2 \int d\bar{\Omega}_x \int ds \frac{\bar{\Omega}_x^2}{(w + 2\bar{\Omega}_x)^{5/2}} e^{-i\bar{\Omega}_x s}. \quad (\text{S28})$$

In this expression, the integrals over $\bar{\Omega}_x$ and s can be computed:

$$\int_0^\infty d\bar{\Omega}_x \int_0^{\bar{t}} ds \frac{\bar{\Omega}_x^2 e^{-i\bar{\Omega}_x s}}{(w + 2\bar{\Omega}_x)^{5/2}} = \left\{ -\bar{t} \sqrt{w(u)} + \frac{1+i}{2} \exp \left[\frac{i}{2} w(u) \bar{t} \right] \sqrt{\pi \bar{t}} (3i - w(u) \bar{t}) \operatorname{erfc} \left[\frac{1+i}{2} \sqrt{\bar{t} w(u)} \right] \right\}, \quad (\text{S29})$$

leading to the function $\mathcal{R}(\bar{t})$ with $\bar{t} = t/t_n$ from the main text.

D Energy for a system in a trap

We compute the contrast for an inhomogeneous density via

$$S(t) = \frac{1}{N} \int d^3 \mathbf{r} S(\mathbf{r}, t) n(\mathbf{r}). \quad (\text{S30})$$

Note that in the homogeneous case the dipolar mean-field energy is zero, but for the trapped case, it does not vanish. In order to evaluate it, we compute

$$E_0(\mathbf{r}) = \int d^3\mathbf{r}' V_{12}(\mathbf{r} - \mathbf{r}') n(\mathbf{r}'), \quad (\text{S31})$$

where $V(\mathbf{r} - \mathbf{r}') = \frac{g_{12}^d}{4\pi|\mathbf{r} - \mathbf{r}'|^3} (\frac{1}{3} - \cos^2 \theta)$ is the DDI interaction in real space. To compute the energy, we employ the convolution theorem,

$$E_0(\mathbf{r}) = \int d^3\mathbf{r}' V_{12}(\mathbf{r} - \mathbf{r}') n(\mathbf{r}) = \mathcal{F}^{-1} \{ \mathcal{F}[V](\mathbf{k}) \mathcal{F}[n](\mathbf{k}) \},$$

where \mathcal{F} and \mathcal{F}^{-1} denote Fourier and Inverse Fourier transforms, respectively. The Fourier transform of the DDI interaction is $\mathcal{F}[V_{12}](\mathbf{k}) = g_{12}^{(d)} (3 \cos^2 \theta_{\mathbf{k}} - 1)$.

Let us assume a Gaussian density profile of a trapped condensate:

$$n(\rho, z) = \frac{N}{\pi^{3/2} l_\rho^2 l_z a_H^3} \exp \left[-\frac{1}{a_H^2} \left(\frac{\rho^2}{l_\rho^2} + \frac{z^2}{l_z^2} \right) \right], \quad (\text{S32})$$

where $a_H = \sqrt{\hbar/m\bar{\omega}}$ is the harmonic oscillator length, $\bar{\omega} = (\omega_\rho^2 \omega_z)^{1/3}$; l_ρ and l_z are variational parameters that depend on the aspect ratio $\lambda = \omega_\rho/\omega_z$. Using that $\mathcal{F}[n](\mathbf{k}) = N \exp \left[-\frac{a_H}{4} (k_\rho^2 l_\rho^2 + k_z^2 l_z^2) \right]$, we write

$$E_0(\mathbf{r}) = \mathcal{F}^{-1} \left[\mathcal{F}^{-1}(V) \mathcal{F}[n](\mathbf{k}) \right] = g_{12}^d N \int \frac{d^3\mathbf{k}}{(2\pi)^3} \left[\frac{3k_z^2}{k_\rho^2 + k_z^2} - 1 \right] \exp \left[-\frac{a_H^4}{4} (k_\rho^2 l_\rho^2 + k_z^2 l_z^2) \right] \exp[-j\mathbf{k} \cdot \mathbf{r}], \quad (\text{S33})$$

or (in dimensionless units):

$$E_0(\mathbf{r}) = \frac{g_{12}^d N}{l_\rho^2 l_z a_H^3} \int \frac{d^3\mathbf{q}}{(2\pi)^3} \left[\frac{3q_z^2}{\Lambda^2 q_\rho^2 + q_z^2} - 1 \right] \exp \left[-\frac{1}{4} (q_\rho^2 + q_z^2) \right] \exp[-j\mathbf{q} \cdot \tilde{\mathbf{r}}], \quad (\text{S34})$$

where $\tilde{\mathbf{r}} = (\tilde{x}, \tilde{y}, \tilde{z}) = \frac{1}{a_H} \left(\frac{x}{l_\rho}, \frac{y}{l_\rho}, \frac{z}{l_z} \right)$ and $\Lambda = l_z/l_\rho$. In spherical coordinates, we write this expression as

$$E_0(\mathbf{r}) = \frac{1}{(2\pi)^3} g_{12}^d N \frac{1}{l_\rho^2 l_z a_H^3} \int dq q^2 \int \sin \theta_q \left[\frac{3 \cos^2 \theta_q}{\Lambda^2 \sin^2 \theta_q + \cos^2 \theta_q} - 1 \right] \exp \left[-\frac{1}{4} q^2 \right] \underbrace{2\pi J_0 \left[q \sin \theta_q \sqrt{\tilde{x}^2 + \tilde{y}^2} \right]}_{\times \exp[-jq \cos \theta_q \tilde{z}] \int_0^{2\pi} d\phi \exp[-jq \sin \theta_q (\tilde{x} \cos \phi + \tilde{y} \sin \phi)]}, \quad (\text{S35})$$

where the integral in ϕ produces a Bessel function J_0 . Using a variable $u = \cos \theta_q$, we write

$$E_0(\mathbf{r}) = \frac{g_{12}^d N}{l_\rho^2 l_z a_H^3} \int \frac{dq}{4\pi^2} \int du q^2 \left[\frac{3u^2}{\Lambda^2 (1 - u^2) + u^2} - 1 \right] J_0 \left[q \sqrt{1 - u^2} \sqrt{\tilde{x}^2 + \tilde{y}^2} \right] e^{-\frac{1}{4} q^2 - jq u \tilde{z}}.$$

We write this expression as

$$E_0(\boldsymbol{\rho}, z) = g_{12}^d n_0 \Omega(\boldsymbol{\rho}, z), \quad \text{where} \quad \Omega(\boldsymbol{\rho}, z) = \int dq \int du f(q, u, \boldsymbol{\rho}, z),$$

$$f(q, u, \boldsymbol{\rho}, z) = \frac{1}{4\sqrt{\pi}} q^2 \left[\frac{3u^2}{\Lambda^2 (1 - u^2) + u^2} - 1 \right] J_0 \left[q \sqrt{1 - u^2} \tilde{\boldsymbol{\rho}} \right] e^{-\frac{1}{4} q^2 - jq u \tilde{z}}.$$

The polaron energy can be conveniently written in the units of energy $E_n = \hbar/t_n = 8\pi\hbar^2 n_0 a_{11}/m$ as

$$\frac{E_0}{E_n}(\boldsymbol{\rho}, z) = \frac{1}{2} \frac{\sqrt{d_1 d_2}}{a_{11}} \Omega(\boldsymbol{\rho}, z). \quad (\text{S36})$$

This quantity is illustrated in Fig. 4 of the main text.

The spatial integral over the energy is known, $\epsilon = \frac{1}{N} \int d^3\mathbf{r} g_{12}^d n_0 \Omega(\boldsymbol{\rho}, z) n(\mathbf{r})$, is known (cf. Ref. [43]). It reads

$$\epsilon = \frac{1}{N} \int d^3\mathbf{r} \int d^3\mathbf{r}' V_{12}(\mathbf{r} - \mathbf{r}') n(\mathbf{r}') n(\mathbf{r}) = \frac{1}{2\sqrt{2}} n_0 g_{12}^d \kappa(\Lambda^{-1}), \quad (\text{S37})$$

where

$$\kappa(\Lambda^{-1}) = \frac{(1 + 2\Lambda^2)}{(\Lambda^2 - 1)} - \frac{3\Lambda^2 \arctan \sqrt{\Lambda^2 - 1}}{(\Lambda^2 - 1)^{3/2}}.$$

References

- [1] T. Langen, R. Geiger and J. Schmiedmayer, *Ultracold atoms out of equilibrium*, Annual Review of Condensed Matter Physics **6**(1), 201 (2015), doi:[10.1146/annurev-conmatphys-031214-014548](https://doi.org/10.1146/annurev-conmatphys-031214-014548).
- [2] R. Citro and F. Mancini, *Out-of-Equilibrium Physics of Correlated Electron Systems*, Springer Series in Solid-State Sciences. Springer International Publishing, ISBN 9783319949567 (2018).
- [3] L. Landau and S. Pekar, *Effective mass of a polaron*, J. Exp. Theor. Phys **18**, 419 (1948).
- [4] J. Devreese and F. Peters, *Polarons and Excitons in Polar Semiconductors and Ionic Crystals*, Plenum Press, New York (1984).
- [5] G. Zhao, *Polarons in Colossal Magnetoresistive and High-Temperature Superconducting Materials*, Alexandrov A.S. (eds) Polarons in Advanced Materials. Springer Series in Materials Science, vol 103 (2007).
- [6] C. Hsieh, J. Liu, C. Duan and J. Cao, *A nonequilibrium variational polaron theory to study quantum heat transport*, The Journal of Physical Chemistry C **123**(28), 17196 (2019), doi:[10.1021/acs.jpcc.9b05607](https://doi.org/10.1021/acs.jpcc.9b05607).
- [7] G. Donati, D. B. Lingerfelt, A. Petrone, N. Rega and X. Li, *Watching polaron pair formation from first-principles electron–nuclear dynamics*, The Journal of Physical Chemistry A **120**(37), 7255 (2016), doi:[10.1021/acs.jpca.6b06419](https://doi.org/10.1021/acs.jpca.6b06419).
- [8] M. Cetina, M. Jag, R. S. Lous, I. Fritsche, J. T. Walraven, R. Grimm, J. Levinsen, M. M. Parish, R. Schmidt, M. Knap and E. Demler, *Ultrafast many-body interferometry of impurities coupled to a Fermi sea*, Science **354**(6308), 96 (2016), doi:[10.1126/science.aaf5134](https://doi.org/10.1126/science.aaf5134).
- [9] M. G. Skou, T. G. Skov, N. B. Jørgensen, K. K. Nielsen, A. Camacho-Guardian, T. Pohl, G. M. Bruun and J. J. Arlt, *Non-equilibrium quantum dynamics and formation of the Bose polaron*, Nature Physics **17**(6), 731 (2021), doi:[10.1038/s41567-021-01184-5](https://doi.org/10.1038/s41567-021-01184-5).
- [10] N. B. Jørgensen, L. Wacker, K. T. Skalmstang, M. M. Parish, J. Levinsen, R. S. Christensen, G. M. Bruun and J. J. Arlt, *Observation of Attractive and Repulsive Polarons in a Bose-Einstein Condensate*, Phys. Rev. Lett. **117**(5), 055302 (2016), doi:[10.1103/PhysRevLett.117.055302](https://doi.org/10.1103/PhysRevLett.117.055302).

- [11] M.-G. Hu, M. J. Van de Graaff, D. Kedar, J. P. Corson, E. A. Cornell and D. S. Jin, *Bose Polarons in the Strongly Interacting Regime*, Phys. Rev. Lett. **117**(5), 055301 (2016), doi:[10.1103/PhysRevLett.117.055301](https://doi.org/10.1103/PhysRevLett.117.055301).
- [12] L. A. Peña Ardila, N. B. Jørgensen, T. Pohl, S. Giorgini, G. M. Bruun and J. J. Arlt, *Analyzing a Bose polaron across resonant interactions*, Phys. Rev. A **99**, 063607 (2019), doi:[10.1103/PhysRevA.99.063607](https://doi.org/10.1103/PhysRevA.99.063607).
- [13] Z. Z. Yan, Y. Ni, C. Robens and M. W. Zwierlein, *Bose polarons near quantum criticality*, Science **368**(6487), 190 (2020), doi:[10.1126/science.aax5850](https://doi.org/10.1126/science.aax5850).
- [14] A. Schirotzek, C.-H. Wu, A. Sommer and M. W. Zwierlein, *Observation of Fermi Polarons in a Tunable Fermi Liquid of Ultracold Atoms*, Phys. Rev. Lett. **102**, 230402 (2009), doi:[10.1103/PhysRevLett.102.230402](https://doi.org/10.1103/PhysRevLett.102.230402).
- [15] M. Koschorreck, D. Pertot, E. Vogt, B. Fröhlich, M. Feld and M. Köhl, *Attractive and repulsive Fermi polarons in two dimensions*, Nature **485**(7400), 619 (2012), doi:[10.1038/nature11151](https://doi.org/10.1038/nature11151).
- [16] C. Kohstall, M. Zaccanti, M. Jag, A. Trenkwalder, P. Massignan, G. M. Bruun, F. Schreck and R. Grimm, *Metastability and coherence of repulsive polarons in a strongly interacting Fermi mixture*, Nature **485**(7400), 615 (2012), doi:[10.1038/nature11065](https://doi.org/10.1038/nature11065).
- [17] F. Scazza, G. Valtolina, P. Massignan, A. Recati, A. Amico, A. Burchianti, C. Fort, M. Inguscio, M. Zaccanti and G. Roati, *Repulsive Fermi Polarons in a Resonant Mixture of Ultracold ^6Li Atoms*, Phys. Rev. Lett. **118**, 083602 (2017), doi:[10.1103/PhysRevLett.118.083602](https://doi.org/10.1103/PhysRevLett.118.083602).
- [18] Y. E. Shchadilova, R. Schmidt, F. Grusdt and E. Demler, *Quantum Dynamics of Ultracold Bose Polarons*, Phys. Rev. Lett. **117**, 113002 (2016), doi:[10.1103/PhysRevLett.117.113002](https://doi.org/10.1103/PhysRevLett.117.113002).
- [19] M. Drescher, M. Salmhofer and T. Enss, *Real-space dynamics of attractive and repulsive polarons in Bose-Einstein condensates*, Phys. Rev. A **99**(2), 664 (2019), doi:[10.1103/PhysRevA.99.023601](https://doi.org/10.1103/PhysRevA.99.023601).
- [20] L. A. P. Ardila, *Dynamical formation of polarons in a Bose-Einstein condensate: A variational approach*, Phys. Rev. A **103**, 033323 (2021), doi:[10.1103/PhysRevA.103.033323](https://doi.org/10.1103/PhysRevA.103.033323).
- [21] A. G. Volosniev, H.-W. Hammer and N. T. Zinner, *Real-time dynamics of an impurity in an ideal Bose gas in a trap*, Phys. Rev. A **92**, 023623 (2015), doi:[10.1103/PhysRevA.92.023623](https://doi.org/10.1103/PhysRevA.92.023623).
- [22] W. E. Liu, Z.-Y. Shi, M. M. Parish and J. Levinsen, *Theory of radio-frequency spectroscopy of impurities in quantum gases*, Phys. Rev. A **102**, 023304 (2020), doi:[10.1103/PhysRevA.102.023304](https://doi.org/10.1103/PhysRevA.102.023304).
- [23] T. Lausch, A. Widera and M. Fleischhauer, *Prethermalization in the cooling dynamics of an impurity in a Bose-Einstein condensate*, Phys. Rev. A **97**, 023621 (2018), doi:[10.1103/PhysRevA.97.023621](https://doi.org/10.1103/PhysRevA.97.023621).
- [24] K. K. Nielsen, L. A. P. Ardila, G. M. Bruun and T. Pohl, *Critical slowdown of non-equilibrium polaron dynamics*, New Journal of Physics **21**(4), 043014 (2019), doi:[10.1088/1367-2630/ab0a81](https://doi.org/10.1088/1367-2630/ab0a81).
- [25] D. Dzsotjan, R. Schmidt and M. Fleischhauer, *Dynamical Variational Approach to Bose Polarons at Finite Temperatures*, Phys. Rev. Lett. **124**, 223401 (2020), doi:[10.1103/PhysRevLett.124.223401](https://doi.org/10.1103/PhysRevLett.124.223401).

- [26] M. Drescher, M. Salmhofer and T. Enss, *Quench Dynamics of the Ideal Bose Polaron at Zero and Nonzero Temperatures*, Phys. Rev. A **103**, 033317 (2021), doi:[10.1103/PhysRevA.103.033317](https://doi.org/10.1103/PhysRevA.103.033317).
- [27] F. Camargo, R. Schmidt, J. D. Whalen, R. Ding, G. Woehl, S. Yoshida, J. Burgdörfer, F. B. Dunning, H. R. Sadeghpour, E. Demler and T. C. Killian, *Creation of Rydberg Polarons in a Bose Gas*, Phys. Rev. Lett. **120**, 083401 (2018), doi:[10.1103/PhysRevLett.120.083401](https://doi.org/10.1103/PhysRevLett.120.083401).
- [28] R. Schmidt, J. D. Whalen, R. Ding, F. Camargo, G. Woehl, S. Yoshida, J. Burgdörfer, F. B. Dunning, E. Demler, H. R. Sadeghpour and T. C. Killian, *Theory of excitation of rydberg polarons in an atomic quantum gas*, Phys. Rev. A **97**, 022707 (2018), doi:[10.1103/PhysRevA.97.022707](https://doi.org/10.1103/PhysRevA.97.022707).
- [29] G. E. Astrakharchik, L. A. P. Ardila, K. Jachymski and A. Negretti, *Many-body bound states and induced interactions of charged impurities in a bosonic bath*, Nature Communications **14**(1) (2023), doi:[10.1038/s41467-023-37153-0](https://doi.org/10.1038/s41467-023-37153-0).
- [30] E. R. Christensen, A. Camacho-Guardian and G. M. Bruun, *Charged Polarons and Molecules in a Bose-Einstein Condensate*, Phys. Rev. Lett. **126**, 243001 (2021), doi:[10.1103/PhysRevLett.126.243001](https://doi.org/10.1103/PhysRevLett.126.243001).
- [31] B. Kain and H. Y. Ling, *Polarons in a dipolar condensate*, Physical Review A **89**(2), 023612 (2014), doi:[10.1103/PhysRevA.89.023612](https://doi.org/10.1103/PhysRevA.89.023612).
- [32] L. A. P. Ardila and T. Pohl, *Ground-state properties of dipolar Bose polarons*, Journal of Physics B: Atomic, Molecular and Optical Physics **52**(1), 015004 (2019), doi:[10.1088/1361-6455/aaf35e](https://doi.org/10.1088/1361-6455/aaf35e).
- [33] F. Schäfer, N. Mizukami and Y. Takahashi, *Feshbach resonances of large-mass-imbalance *er-li* mixtures*, Phys. Rev. A **105**, 012816 (2022), doi:[10.1103/PhysRevA.105.012816](https://doi.org/10.1103/PhysRevA.105.012816).
- [34] F. Schäfer, Y. Haruna and Y. Takahashi, *Realization of a quantum degenerate mixture of highly magnetic and nonmagnetic atoms*, Phys. Rev. A **107**, L031306 (2023), doi:[10.1103/PhysRevA.107.L031306](https://doi.org/10.1103/PhysRevA.107.L031306).
- [35] M. Lu, N. Q. Burdick and B. L. Lev, *Quantum degenerate dipolar fermi gas*, Phys. Rev. Lett. **108**, 215301 (2012), doi:[10.1103/PhysRevLett.108.215301](https://doi.org/10.1103/PhysRevLett.108.215301).
- [36] A. Trautmann, P. Ilzhöfer, G. Durastante, C. Politi, M. Sohmen, M. J. Mark and F. Ferlaino, *Dipolar Quantum Mixtures of Erbium and Dysprosium Atoms*, Phys. Rev. Lett. **121**(21), 213601 (2018), doi:[10.1103/PhysRevLett.121.213601](https://doi.org/10.1103/PhysRevLett.121.213601).
- [37] G. Durastante, C. Politi, M. Sohmen, P. Ilzhöfer, M. J. Mark, M. A. Norcia and F. Ferlaino, *Feshbach resonances in an erbium-dysprosium dipolar mixture*, Phys. Rev. A **102**, 033330 (2020), doi:[10.1103/PhysRevA.102.033330](https://doi.org/10.1103/PhysRevA.102.033330).
- [38] L. Santos, G. V. Shlyapnikov and M. Lewenstein, *Roton-Maxon Spectrum and Stability of Trapped Dipolar Bose-Einstein Condensates*, Phys. Rev. Lett. **90**, 250403 (2003), doi:[10.1103/PhysRevLett.90.250403](https://doi.org/10.1103/PhysRevLett.90.250403).
- [39] L. Chomaz, R. M. W. van Bijnen, D. Petter, G. Faraoni, S. Baier, J. H. Becher, M. J. Mark, F. Wächtler, L. Santos and F. Ferlaino, *Observation of roton mode population in a dipolar quantum gas*, Nature Physics **14**(5), 442 (2018), doi:[10.1038/s41567-018-0054-7](https://doi.org/10.1038/s41567-018-0054-7).

- [40] L. Chomaz, I. Ferrier-Barbut, F. Ferlaino, B. Laburthe-Tolra, B. L. Lev and T. Pfau, *Dipolar physics: a review of experiments with magnetic quantum gases*, Reports on Progress in Physics **86**(2), 026401 (2022), doi:[10.1088/1361-6633/aca814](https://doi.org/10.1088/1361-6633/aca814).
- [41] F. Böttcher, J.-N. Schmidt, J. Hertkorn, K. S. H. Ng, S. D. Graham, M. Guo, T. Langen and T. Pfau, *New states of matter with fine-tuned interactions: quantum droplets and dipolar supersolids*, Reports on Progress in Physics **84**(1), 012403 (2020), doi:[10.1088/1361-6633/abc9ab](https://doi.org/10.1088/1361-6633/abc9ab).
- [42] H. S. Adlong, W. E. Liu, F. Scazza, M. Zaccanti, N. D. Oppong, S. Fölling, M. M. Parish and J. Levinsen, *Quasiparticle Lifetime of the Repulsive Fermi Polaron*, Phys. Rev. Lett. **125**, 133401 (2020), doi:[10.1103/PhysRevLett.125.133401](https://doi.org/10.1103/PhysRevLett.125.133401).
- [43] T. Lahaye, C. Menotti, L. Santos, M. Lewenstein and T. Pfau, *The physics of dipolar bosonic quantum gases*, Reports on Progress in Physics **72**(12), 126401 (2009), doi:[10.1088/0034-4885/72/12/126401](https://doi.org/10.1088/0034-4885/72/12/126401).
- [44] G. Bighin, A. Burchianti, F. Minardi and T. Macrì, *Impurity in a heteronuclear two-component Bose mixture*, Phys. Rev. A **106**, 023301 (2022), doi:[10.1103/PhysRevA.106.023301](https://doi.org/10.1103/PhysRevA.106.023301).
- [45] P. Kramer and M. Saraceno, *Geometry of the time-dependent variational principle in quantum mechanics*, Lecture notes in physics. Springer (1981).
- [46] T. D. Lee, F. E. Low and D. Pines, *The motion of slow electrons in a polar crystal*, Phys. Rev. **90**, 297 (1953), doi:[10.1103/PhysRev.90.297](https://doi.org/10.1103/PhysRev.90.297).
- [47] M. G. Skou, T. G. Skov, N. B. Jørgensen and J. J. Arlt, *Initial Dynamics of Quantum Impurities in a Bose–Einstein Condensate*, Atoms **9**(2) (2021), doi:[10.3390/atoms9020022](https://doi.org/10.3390/atoms9020022).
- [48] M. G. Skou, K. K. Nielsen, T. G. Skov, A. M. Morgen, N. B. Jørgensen, A. Camacho-Guardian, T. Pohl, G. M. Bruun and J. J. Arlt, *Life and death of the Bose polaron*, Phys. Rev. Res. **4**, 043093 (2022), doi:[10.1103/PhysRevResearch.4.043093](https://doi.org/10.1103/PhysRevResearch.4.043093).
- [49] R. N. Bisset, L. A. P. Ardila and L. Santos, *Quantum Droplets of Dipolar Mixtures*, Phys. Rev. Lett. **126**, 025301 (2021), doi:[10.1103/PhysRevLett.126.025301](https://doi.org/10.1103/PhysRevLett.126.025301).
- [50] D. Scheiermann, L. A. P. Ardila, T. Bland, R. N. Bisset and L. Santos, *Catalyzation of supersolidity in binary dipolar condensates*, Phys. Rev. A **107**, L021302 (2023), doi:[10.1103/PhysRevA.107.L021302](https://doi.org/10.1103/PhysRevA.107.L021302).
- [51] S. Li, U. N. Le and H. Saito, *Long-lifetime supersolid in a two-component dipolar bose-einstein condensate*, Phys. Rev. A **105**, L061302 (2022), doi:[10.1103/PhysRevA.105.L061302](https://doi.org/10.1103/PhysRevA.105.L061302).
- [52] J. Sanchez-Baena, C. Politi, F. Maucher, F. Ferlaino and T. Pohl, *Heating a quantum dipolar fluid into a solid* (2022), [2209.00335](https://arxiv.org/abs/2209.00335).
- [53] A. Camacho-Guardian, L. A. P. Ardila, T. Pohl and G. M. Bruun, *Bipolarons in a Bose-Einstein Condensate*, Phys. Rev. Lett. **121**(1), 013401 (2018), doi:[10.1103/PhysRevLett.121.013401](https://doi.org/10.1103/PhysRevLett.121.013401).
- [54] G. Panochko and V. Pastukhov, *Two- and three-body effective potentials between impurities in ideal BEC*, Journal of Physics A: Mathematical and Theoretical **54**(8), 085001 (2021), doi:[10.1088/1751-8121/abdbc5](https://doi.org/10.1088/1751-8121/abdbc5).
- [55] G. Bighin, P. A. Murthy, N. Defenu and T. Enss, *Resonantly enhanced superconductivity mediated by spinor condensates*, doi:[10.48550/ARXIV.2212.07419](https://doi.org/10.48550/ARXIV.2212.07419) (2022).

- [56] S. I. Mistakidis, A. G. Volosniev and P. Schmelcher, *Induced correlations between impurities in a one-dimensional quenched Bose gas*, Phys. Rev. Res. **2**, 023154 (2020), doi:[10.1103/PhysRevResearch.2.023154](https://doi.org/10.1103/PhysRevResearch.2.023154).
- [57] G. Wang, A. Chernikov, M. M. Glazov, T. F. Heinz, X. Marie, T. Amand and B. Urbaszek, *Colloquium: Excitons in atomically thin transition metal dichalcogenides*, Rev. Mod. Phys. **90**, 021001 (2018), doi:[10.1103/RevModPhys.90.021001](https://doi.org/10.1103/RevModPhys.90.021001).
- [58] S. Yi and L. You, *Trapped atomic condensates with anisotropic interactions*, Phys. Rev. A **61**, 041604 (2000), doi:[10.1103/PhysRevA.61.041604](https://doi.org/10.1103/PhysRevA.61.041604).
- [59] D. C. E. Bortolotti, S. Ronen, J. L. Bohn and D. Blume, *Scattering Length Instability in Dipolar Bose-Einstein Condensates*, Phys. Rev. Lett. **97**, 160402 (2006), doi:[10.1103/PhysRevLett.97.160402](https://doi.org/10.1103/PhysRevLett.97.160402).
- [60] S. Ronen, D. C. E. Bortolotti, D. Blume and J. L. Bohn, *Dipolar Bose-Einstein condensates with dipole-dependent scattering length*, Phys. Rev. A **74**, 033611 (2006), doi:[10.1103/PhysRevA.74.033611](https://doi.org/10.1103/PhysRevA.74.033611).
- [61] E. Braaten and H.-W. Hammer, *Universality in few-body systems with large scattering length*, Physics Reports **428**(5), 259 (2006), doi:<https://doi.org/10.1016/j.physrep.2006.03.001>.